LA-UR-01-5650
*Approved for public release; distribution is unlimited.*

*Title:* **BOLIDE PHYSICAL THEORY WITH APPLICATION TO PN AND EN FIREBALLS**

*Author(s):* D. O. ReVelle and Z. Ceplecha

*Submitted to:*

http://lib-www.lanl.gov/la-pubs/00796548.pdf

# BOLIDE PHYSICAL THEORY WITH APPLICATION TO PN AND EN FIREBALLS

**D. O. ReVelle[(1)] and Z. Ceplecha[(2)]**

*[(1)]Los Alamos National Laboratory, P.O. Box 1663, MS J577, Earth and Environmental Sciences Division, EES-8, Atmospheric and Climate Science Group, Los Alamos, NM 87545, USA, Email: dor@vega.lanl.gov*
*[(2)]Emeritus: Academy of Sciences, Astronomical Institute, Observatory, 25165 Ondřejov*

## ABSTRACT

Using data on 22 "precise bolides" with up to 882 individual points on their trajectories [4], [5], and using data on 29 "bright bolides" and on 10 artificial meteors [6], [8], [9], [10], we tried to derive dependence of ablation and shape-density coefficients, and of luminous efficiency on various time dependent parameters. The only significant dependence we found was that on $v_\infty - v$ (on difference of initial and instantaneous velocities). We present the results as Eq. 3, 4 and 8, with coefficients $a_1, a_2, a_3, a_4, b_1, b_2, b_3, c_1, c_2$ computed for different bolide types. Also average values of ablation, and shape-density coefficients as well as average luminous efficiencies for individual bolide types are given.

## 1. BASIC DIFFERENCIAL EQUATIONS

Basic differential equations of meteor motion, ablation and radiation are given in [1]. The geometrical conditions of a bolide trajectory are described as a straight line over the local spherical Earth's surface. The shape-density coefficient, $K$, the ablation coefficient, $\sigma$, and the luminosity coefficient, $\tau$, are defined also in [1] (page 349).

## 2. SOLUTION WITH CONSTANT COEFFICIENTS

Solutions with constant coefficients $K$ and $\sigma$ ([1], [2], [3]) applied to sufficiently precise data (better than ±30 m for one observed distance along the trajectory) on photographic multistation bolides yielded about 40% fits without gross-fragmentation, and about 40% fits with one gross-fragmentation point. The rest are either events with multi-fragmentation or with coefficients $K$ and $\sigma$ variable with time. Thus we need to proceed to a solution of the basic differential equations with $K$ and $\sigma$ being variable with time.

## 3. SOLUTIONS WITH VARIABLE COEFFICIENTS

Solution of the basic equations with $K$ and $\sigma$ being a general function of time is given in [4]. This solution was applied to 22 bolides (PN and Ondřejov) with precision mostly around ±10 m for one measured distance along trajectory (extremes were between ±4 m and ±15 m). For shortness we will refer to these 22 bolides as to "precise bolides". The results on precise bolides are given in [4], and in details in [5] (267 individual plots of different parameters for "precise bolides" as function of time).

## 4. DEPENDENCE OF ABLATION COEFFICIENT, σ, ON PARAMETERS

A suitable analysis of precise bolides could yield dependence of $\sigma$ on time dependent parameters. We performed the analysis for type-I and for type-II bolides separately. We have not enough data to do the analysis for type-IIIA bolides and type-IIIB bolides, thus for these two groups the average $\sigma$-values stay the only available.

The data on $\sigma$ for "precise bolides" in [4] were used to derive the change of $\sigma$ with various parameters. We limited ourselves to search for coefficients of logarithmic additive dependences, which is equivalent to multiplication of parameters, each put on an unknown power. This procedure of deriving dependence of $\sigma$ on any chosen parameter, $P$, can be described by Eq. 1. If any chosen parameter is denoted $P$, then we can define relation of $\ln P$ to $\ln \sigma$ ($\ln$ is the natural logarithm) as

$$\ln \sigma_i = a_1 \ln P + a_{(i+1)} \quad , \quad i = 1, 2, \ldots , n \qquad (1)$$

where $n$ is the number of different bolides we used for computation. Because we have many values available for each of the $i$-th bolide, we can use the

least squares solution of Eq. 1. Then $a_1$ defines the average slope in the $\ln\sigma$ over $\ln P$ for all bolides used, while the values of $a_2$ until $a_{(n+1)}$ are shifts of individual dependences according to the average $\ln\sigma$ value. We have available 391 individual values of $\sigma$ for 15 type-II bolides. Results derived from these data: $\sigma$ does not depend on $m, \frac{\mathrm{d}m}{\mathrm{d}t}, h$. However, $\sigma$ depends on $v, \frac{\mathrm{d}v}{\mathrm{d}t}$ as:

$$\sigma \propto v^{-0.63\pm0.12}\left(-\frac{\mathrm{d}v}{\mathrm{d}t}\right)^{-0.32\pm0.05} \qquad (2)$$

The proportionality constant in (2) resulted from (1) with standard deviation larger than its value. Inspecting the reasons we came to the conclusion that relation (2) originates in dependence of $\sigma$ on $v_\infty - v$ (where $v_\infty$ is the initial velocity). Relation of $\sigma$ and $v_\infty - v$ was the strongest dependence we were able to find and also with the least residuals. Individual values of $\ln\sigma$ for each bolide were corrected to the same level of average $\sigma$ = 0.042 s$^2$ km$^{-2}$ using the values $a_2$ until $a_{(1+n)}$. The resulting average values of $\ln\sigma$ for type-II bolides and for different intervals of $\ln(v_\infty - v)$ are summarized in Table 1 and plotted in Fig.1. The interval limits applied were 0, 0.5, 0.8, 0.9, 1.1, 1.25, 1.55, 1.0, defining 9 intervals. The smooth curve in Fig. 1 is the best fit to the average values by using a function defined as

$$\ln\sigma = a_1 \exp\{a_2\,[\ln(v_\infty - v) + a_3]^2\} + a_4 \qquad (3)$$

The best fit for the type-II bolides corresponds to
$a_1 = -0.84,\ a_2 = -4.67,\ a_3 = -0.88,\ a_4 = -2.86$
Standard deviation of the fit for one point is $\pm0.08$ in $\ln\sigma$.

There is not much data available on the „exact bolides“ of type I to do the same analysis as for type-II bolides. We have only 56 individual values of $\ln\sigma$ belonging to 4 different bolides available. Again we used corrections of $\ln\sigma$ to the same average level (type-I, i.e. $\sigma$ = 0.014 s$^2$ km$^{-2}$ ), and also no other significant dependence than that on $\ln(v_\infty - v)$ was found. The resulting average values of $\ln\sigma$ for type-I bolides and for different intervals of $\ln(v_\infty - v)$ are summarized in Table 2 and plotted in Fig. 1. The interval limits applied were 0.72, 1.04, 1.50, 1.78, defining five intervals. Because we have only 56 points divided into 5 intervals, it was not possible to determine all 4 unknown parameters of Eq. (3) just

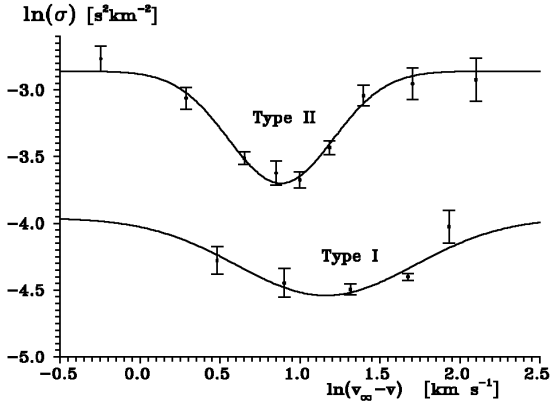


Fig. 1.

from these data alone. We used an additional condition that $\ln\sigma$ for very large and very small values of $\ln(v_\infty - v)$ have to be –3.96, i.e. a value that keeps the average difference of $\ln\sigma$ between type-I and type-II bolides equal to 1.10, which corresponds to $\sigma$-ratio 1 to 3 (0.014 to 0.042). The smooth curve in Fig. 1 for the type-I bolides is the best fit of Eq. 3 to values in Table 1 and corresponds to
$a_1 = -0.58, a_2 = -1.60, a_3 = -1.16, a_4 = -3.96$.
Standard deviation for one point is $\pm0.03$ in $\ln\sigma$. This reflects the situation that we determined only 3 unknowns (the fourth one was fixed at –3.96).

Table 1. Type-II bolides
n … is number of individual values

| $\ln(\sigma)$ | $\ln(v_\infty - v)$ | n |
|---|---|---|
| -2.767 ±0.094 | –0.247 ±0.030 | 38 |
| -3.062 ±0.081 | 0.287 ±0.021 | 52 |
| -3.512 ±0.048 | 0.651 ±0.010 | 68 |
| -3.623 ±0.092 | 0.850 ±0.006 | 23 |
| -3.675 ±0.059 | 0.998 ±0.009 | 45 |
| -3.432 ±0.052 | 1.184 ±0.008 | 32 |
| -3.043 ±0.077 | 1.396 ±0.012 | 52 |
| -2.954 ±0.120 | 1.703 ±0.015 | 54 |
| -2.925 ±0.162 | 2.100 ±0.035 | 27 |

Table 2. Type-I bolides
n … is number of individual values

| $\ln(\sigma)$ | $\ln(v_\infty - v)$ | n |
|---|---|---|
| -4.278 ±0.103 | 0.482 ±0.049 | 12 |
| -4.446 ±0.107 | 0.901 ±0.029 | 10 |
| -4.494 ±0.042 | 1.315 ±0.043 | 10 |
| -4.400 ±0.026 | 1.674 ±0.023 | 9 |
| -4.024 ±0.123 | 1.931 ±0.024 | 15 |

## 5. DEPENDENCE OF SHAPE–DENSITY COEFFICIENT, *K*, ON PARAMETERS

The 22 „precise bolides“ were used to derive the change of $K$ with various parameters. The procedure of doing so was the same as described for σ using Eq. (1). We also corrected individual $K$ values for the average $K$ of the corresponding type (type I: average $K$=0.46, type II: average $K$=0.69 ). We have available substantially more individual values of $K$ than those of σ, we used for determining average dependence of σ on different parameters. This situation reflects the fact that σ cannot be determined at the early parts of trajectories, and $K$ moreover does not depend on the average σ used at these early parts of trajectories. Thus we have available 882 individual values of $K$ for type-II bolides. We tested the dependence of these 882 values of $K$ on $v$, $\mathrm{d}v/\mathrm{d}t$, $m$, $\mathrm{d}m/\mathrm{d}t$ and $h$. No significant dependence (i.e. exceeding one standard deviation) was found. Particularly, $K$ proved to be independent of height $h$ (i.e. of the air density).

We also added the difference of $v_\infty - v$ to possible parameters, because $K$ shows a well defined and rather strong dependence on this parameter. Applying Eq. (5) (the least-squares) to all 15 bolides available for type-II "precise bolides", we found a strong correlation to $v_\infty - v$. Using the 882 values mentioned above, we computed averages of $\ln(v_\infty - v)$ and $\ln K$ for consecutive intervals of $\ln(v_\infty - v)$ chosen so that the standard deviations of average values of $\ln K$ were kept in reasonable limits. The interval limits we applied were –3.5, –1.5, –1.0, –0.5, –0.1, 0.3, 0.7, 1.1, 1.5, defining 9 intervals (we omitted 3 points with $\ln(v_\infty - v) < -3.5$, because of a very large spread due to large standard deviations of individual values). The results are given in Table 3 and Fig. 2. The smooth curve in Fig. 2 is the best fit of a function defined as:

$$\ln K = b_1 + b_2 \tanh(b_3 \ln(v_\infty - v)) \qquad (4)$$

The fit for type-II bolides corresponds to
$b_1 = -0.3,\ \ b_2 = 2.5,\ \ b_3 = -0.2$.
Standard deviation for one point is ±0.11 in $\ln K$. All this is already with correction to average value of $\ln K$. The average value of $\ln K$ computed from Eq. (4) with the above given values of $b_1, b_2, b_3$, and computed inside an interval of $\ln(v_\infty - v)$ from –2.3 to 2.6 resulted as $\ln K = -0.37$, i.e. $K = 0.69$ (c.g.s.).

There is not much data available on the "precise bolides" of type I, but it is again more than for determining average dependence of σ on parameters.

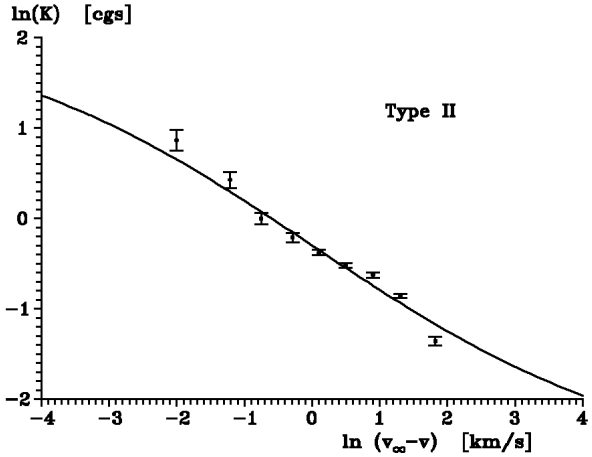

Fig. 2.

The variability of $\ln K$ with different time dependent parameters was tested by means of all 4 "precise bolides" of type I. Altogether we have available 124 values of $K$ for type I. Using these 124 values, we computed averages of $\ln(v_\infty - v)$ and $\ln K$ for consecutive intervals of $\ln(v_\infty - v)$ chosen so that the standard deviations of average values of $\ln K$ were kept in reasonable limits. The interval limits we applied were –0.5, 0.5, 1.5, defining 4 intervals. The results are given in Table 4. These values are very close to the smooth curve in Fig. 2 (derived for type-II bolides). The average $\ln K$ = –0.776, i.e. $K$ = 0.46 (c.g.s), i.e. exactly the average value for all PN bolides. This corresponds to interval from -1.6 to 3.6 in $\ln(v_\infty - v)$, if equation (4) is used with the same values of $b_1, b_2, b_3$, as it was derived for type-II bolides. Because of not enough precision, our conclusion is simple. There is no significant (one standard deviation) difference of $\ln K$ as function of $\ln(v_\infty - v)$ from the dependence derived for type-II bolides. Thus we will assume that this function is the same for type-I as well as for type-II bolides.

Table 3. Type-II bolides
n … is number of individual values

| $\ln K$ | $\ln(v_\infty - v)$ | n |
|---|---|---|
| 0.865 ± 0.113 | -2.005 ± 0.041 | 75 |
| 0.426 ± 0.088 | -1.213 ± 0.017 | 77 |
| -0.002 ± 0.061 | -0.752 ± 0.015 | 107 |
| -0.211 ± 0.051 | -0.289 ± 0.012 | 96 |
| -0.379 ± 0.029 | 0.099 ± 0.012 | 93 |
| -0.520 ± 0.026 | 0.496 ± 0.012 | 95 |
| -0.628 ± 0.028 | 0.901 ± 0.012 | 98 |
| -0.858 ± 0.024 | 1.307 ± 0.010 | 126 |
| -1.358 ± 0.049 | 1.821 ± 0.024 | 112 |

Table 4. Type-I bolides
n … is number of individual values

| $\ln K$ | $\ln(v_\infty - v)$ | n |
|---|---|---|
| –0.122 ± 0.115 | –0.888 ± 0.063 | 26 |
| –0.830 ± 0.071 | 0.048 ± 0.054 | 29 |
| –0.831 ± 0.045 | 0.975 ± 0.051 | 32 |
| –1.192 ± 0.029 | 1.924 ± 0.036 | 33 |

## 6. DEPENDENCE OF LUMINOUS EFFICIENCY, τ, ON PARAMETERS

The entire section on luminous efficiency will deal exclusively with the *differential* luminous efficiency, τ, as defined in [1] (page 362, eq. (29)). The average values of τ for individual bolide types can be derived from a previous study on "bright bolides" in [6], where all the needed data are contained in Table 2, and where the whole procedure of computing and correcting one average value of τ for each bolide is described on pages 48 to 50. The results based on 29 individual "bright bolides" are given in Table 5 together with the average values of $K$ and σ (τ is given in percents of total kinetic energy, $E$ ). There was not enough data available for obtaining independent values of τ for type IIIA and IIIB separately, and they were treated as one group.

Table 5: Average values of $K$, σ and τ for different bolide types:
( τ is in percent of total kinetic energy, $E$ )

| type | I | II | IIIA | IIIB |
|---|---|---|---|---|
| $\rho_d$ g cm$^{-3}$ | 3.7 | 2.0 | 0.75 | 0.27 |
| σ s$^2$ km$^{-2}$ | 0.014 | 0.042 | 0.10 | 0.21 |
| $K$ cgs (ΓA=1.1) | 0.46 | 0.69 | 1.33 | 2.63 |
| τ % of $E$ | 5.57 | 1.35 | 0.242 | |

### 6.1 Luminous Efficiency as Function of Velocity and Mass

Since the very beginning of meteor physics, it was recognized that luminous efficiency depends on velocity. We start the present analysis with a function given in [7] (Fig.1 and equation (40)). Below 16 km/s the cited relation took into account experimental results (artificial meteors produced in the atmosphere by man-made bodies fired down from high altitude rockets) given in [8], and also results given in [9] based on detailed study of motion of individual recovered fragments of the Innisfree meteorite (photographic records available). The relation can be written as an interpolation formula (already in a form using natural logarithms) :

for $v < 25.372$ km/s:

$$\ln\tau = k_1 - 10.307\ln v + 9.781(\ln v)^2 - 3.0414(\ln v)^3 + 0.3213(\ln v)^4 \qquad (5)$$

for $v \geq 25.372$ km/s:

$$\ln\tau = \ln v + k_2$$

where values of $k_1 = -1.494$ and $k_2 = -3.488$ correspond to the values in the cited paper. However, we will left $k_1$ and $k_2$ as free parameters, and determine their numerical values for individual bolide types after we enlarge the expression (5) by additional terms for mass, $m$, and eventually by additional terms for other possible parameters.

What remains to be done first is the dependence of τ on mass, which came forward as being possible after the analysis of the Lost City bolide and meteorite fall was published in [10]. Well documented meteorite falls (multistation photographic records) form a reliable way to gain realistic values of τ , because the dynamical mass computations can be calibrated by the terminal mass (recovered meteorites). Such results seem to be equivalent to the results of the rocket experiments in [8], and moreover yield data on much larger bodies and also somewhat speedier. We used the following expression of τ–dependence on mass as an additive term to the velocity dependence:

$$\ln\tau(m) = k_3 + k_3 \tanh(k_4 \ln m) \qquad (6)$$

If Eq. (6) is used as an additive term to Eq. (5), the advantage of a smooth change of τ with $m$ between two extreme values (one for very small masses and the other for very large masses) is evident. The form of Eq. (6) assumes that the largest change of τ with $m$ takes place at masses of 1 kg, which corresponds to the situation that experimental values for smaller masses of several grams in [8] are about 10× smaller than the values derived for the Lost City meteoroid (initial mass

Fig. 3.

of 163 kg). These two sets of $\tau$ values, the Innisfree bolide $\tau$–values for different fragments, and the

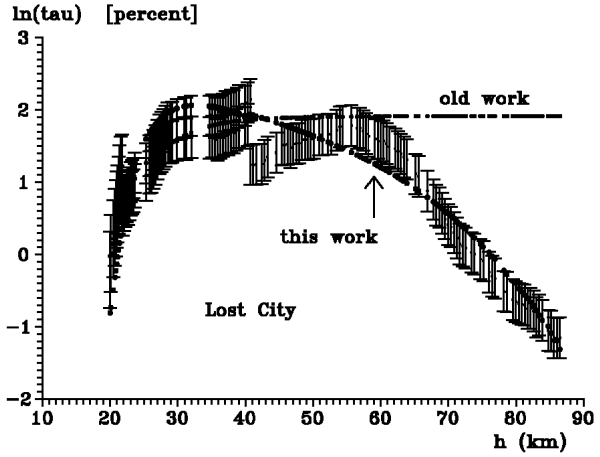


„bright bolide“ $\tau$–values were normalized to the same velocity by Eq. (5). Then Eq. (6) applied to them yielded $k_3 = 1.15 \pm 0.16$, and $k_4 = 0.38 \pm 0.12$.

### 6.2 Luminous Efficiency as Function of Other Parameters

Data on 15 „precise bolides“ (those for which photometric data are available) can be used the same way as we already have used data on all 22 „precise bolides“ for determining dependence of $\sigma$ and $K$ on different parameters. Similar procedure as described by Eq. (1) was adopted to residuals

$$\ln \tau\,(\text{obs}) - \ln \tau\,(\text{com}) ,$$

where the computed values of $\ln \tau$ included sum of both $\ln \tau$ values computed from equation (5) and (6). The individual values of $\ln \tau$ at all 791 observed points of 15 „precise bolides“ were used as the observed values of $\ln \tau$. No significant dependence on different parameters were found except for $\ln(v_\infty - v)$ (this is in analogy to the previous $\sigma$ and $K$ results). The resulting dependence of the above defined residuals on $\ln(v_\infty - v)$ was found as

$$\ln \tau = k_5 + k_6 \ln(v_\infty - v) + k_7 (\ln(v_\infty - v))^3 \quad (7)$$

where the fit to 791 values of residuals yielded $k_6 = 0.26 \pm 0.02$ and $k_7 = 0.0042 \pm 0.0005$, while $k_5$ for individual bolides differed so much that its standard deviation is well outside its average value.

### 6.3 Resulting Expression for Computing Luminous Efficiency for Different Bolide Types

If we add all terms (5), (6), and (7), we receive only two constants, $c_1$ and $c_2$, valid for two different velocity intervals defined by (5): $c_1 = k_1 + k_3 + k_5$ and $c_2 = k_2 + k_3 + k_5$. These two constants differ for different bolide types and were determined using equation (8) so that the average difference of $\ln \tau$ follows the differences given in Table 5. The resulting expression for computing $\ln \tau$ is given as follows

for $v < 25.372$ km/s

$$\ln \tau = c_1 - 10.307 \ln v + 9.781 (\ln v)^2 - 3.0414 (\ln v)^3 + 0.3213 (\ln v)^4 + 1.15 \tanh(0.38 \ln m) + 0.26 \ln(v_\infty - v) + 0.0042 (\ln(v_\infty - v))^3 \quad (8)$$

for $v \geq 25.372$ km/s

$$\ln \tau = c_2 + \ln v + 1.15 \tanh(0.38 \ln m) + 0.26 \ln(v_\infty - v) + 0.0042 (\ln(v_\infty - v))^3$$

where

for type-I bolides $c_1 = +0.466,\ c_2 = -1.538$

for type-II bolides $c_1 = -0.955,\ c_2 = -2.959$

for type-IIIA , IIIB $c_1 = -2.670,\ c_2 = -4.674$

When the resulting Eq. (8) was used for the Lost City bolide, and the computed values of $\ln \tau$ compared to those values previously derived in [10], a significant improvement was evident. Especially luminous efficiencies determined for the early parts of the Lost City trajectory were not explainable by the previous analysis of $\tau$ (not having the “precise bolide” data available at that time). However, $\ln \tau$ of the present analysis fits quite well also to the observed values of $\ln \tau$ for the early parts of the Lost City bolide. This improvement was induced into the final expression (8) by the analysis of the „precise bolides“. A comparison of the old and the new values of $\ln \tau$ for Lost City bolide is presented in Fig. 3 and forms an independent evidence that the present analysis of $\ln \tau$ is principally correct.

### 6.4 Radiation Pass-Band of the Derived Luminous Efficiency

For deriving $\tau$ in this section, we made use of data on luminosity obtained from photographic observations with panchromatic emulsions. Thus the derived $\tau$–values correspond to panchromatic pass-band, i.e. approximately between 360 and 650 nm. However, most of bolide energy, especially for slower meteoroids, is radiated just in this pass-band with characteristic temperature of 4500 K for the main spectral component (in [1], page 362–366). Spectral data on radiation in another pass-bands are almost missing. Had them available we could derive spectral (temperature) corrections to values of Eq.(8), transforming $\tau$ to other spectral pass-bands.

### 6.5 Comparison to Earlier Theoretical Work

In [11], the panchromatic luminous efficiency was explicitly calculated for the three photographed and recovered meteorites, Lost City, Innisfree and Pribram using the entry model in [12] using the luminous efficiency equation expressed in terns of the full kinetic energy depletion process. The calculations for all three meteorites all indicated a nearly Gaussian shaped pulse of the luminous efficiency versus height whose peak value was ~ 1-2 %, with the exception of the more uncertain case of Pribram which was not observed photographically at all altitudes. The degree to which the current approach agrees with these earlier results is far better than we could have expected, especially since the new results were done totally independently from the earlier work. It is especially of interest that these two approaches agree so well, both in shape and in the magnitude of the luminous efficiency since the two approaches are so different. The approach in [11] and in [12] produces results based on the observed bolide flight data and very detailed physically based convective and radiative transfer calculations (with the latter being the dominant heat transfer mechanism for large bodies). The current approach has only flight data at its disposal, including the historically difficult to measure deceleration, since it depends on a time derivative of the directly observed velocity. The excellent agreement between these two approaches is clearly a topic that should be more fully investigated.

## 7. REFERENCES


1..Ceplecha Z., Borovička J., Elford W.G., ReVelle D.O., Hawkes R.L., Porubčan V., and Šimek M., Meteor Phenomena and Bodies, *Space Science Reviews,* Vol. 84, 327–471, 1998

2. Ceplecha Z., Spurný P., Borovička J., and Keclíková J., Atmospheric Fragmentation of Meteoroids, *Astron. Astrophys.,* Vol. 279, 615–626, 1993.

3. Ceplecha Z., Meteoroid Properties from photographic Records of Meteors and Fireballs, Asteroids, Comets, Meteors 1993, *IAU Symp.* 160, 343–356, 1994.

4. Ceplecha Z., Borovička J., and Spurný P., Dynamical Behavior of Meteoroids in the Atmosphere Derived from Very Precise Photographic Records, *Astron. Astrophys.* Vol. 367,1115–1122, 2000.

5. Ceplecha Z., Borovička J., and Spurný P., Dynamical Behavior of Meteoroids in the Atmosphere Derived from Very Precise Photographic Records, Plots for Results, http://www.asu.cas.cz/~ceplecha/precbol.html,2000.

6. Ceplecha Z., Spalding R.E., Jacobs C. and Tagliaferri E., Luminous Efficiencies of Bolides, *Proc. SPIE*, Vol. 2813, 46–56, 1996.

7. Pecina P. and Ceplecha Z., New Aspects in Single-Body Meteor Physics, *Bull. Astron. Inst. Czech.*, Vol. 34, 120–121, 1983.

8. Ayers W.G., McCrosky R.E., and Shao C.-Y., Photographic Observations of 10 Artificial Meteors, *Smithsonian Astrophys. Obs. Spec. Rep.*, Vol. 317, 1–40, 1970.

9. Halliday I., Griffin A.A., and Blackwell A.T., The Innisfree Meteorite Fall, *Meteoritics* Vol. 16, 153–170, 1981.

10. Ceplecha Z., Luminous Efficiency Based on Photographic Observations of the Lost City Fireball and Implication for the Influx of Interplanetary Bodies onto Earth, *Astron. Astrophys.* Vol. 311, 329–332, 1996.

11. ReVelle, D.O. and R.S. Rajan (1979), On the Luminous Efficiency of Meteoritic Fireballs, J. Geophysical Research, 84, 6255-6262, 1979.

12. ReVelle, D.O., A Quasi-simple Ablation Model for Large Meteorite Entry: Theory versus Observations, J. Atmospheric Terrestrial Physics, 41, 453-473, 1979.